Supplemental Material to DNA-stabilized Ag–Au bimetallic clusters: The effect of alloying and embedding on optical properties

Dennis Palagin* and Jonathan P. K. Doye

CONTENTS

* dennis.palagin@chem.ox.ac.uk

SI. INFLUENCE OF THE VAN DER WAALS DISPERSION CORRECTION

We have re-calculated the adsorption energies presented in Table I of the manuscript (binding energies for pure and alloyed clusters with two cytosine bases) by including the Tkatchenko-Scheffler dispersion correction [S1] as implemented in the CASTEP suite. The comparison of the adsorption energy values for the structures with and without the dispersion correction can be found in the following table:

Structure	Adsorption energy, eV	
	no vdW	including vdW correction
C–Ag_4–C	1.79	2.06
C–Ag_6–C	1.13	1.24
C–Ag_8–C	1.06	1.38
C–Ag_{10}–C	1.32	1.65
C–Ag_{12}–C	1.34	1.63
C–Ag_2Au_2–C	1.92	2.14
C–Ag_3Au_3–C	1.23	1.31
C–Ag_4Au_4–C	1.42	1.57
C–Ag_5Au_5–C	1.66	1.81
C–Ag_6Au_6–C	1.42	1.58
C–Au_4–C	2.46	2.66
C–Au_6–C	1.59	1.69
C–Au_8–C	2.26	2.34
C–Au_{10}–C	1.75	2.03
C–Au_{12}–C	1.89	2.01

TABLE SI. Binding energies for pure and alloyed clusters with two cytosine bases, calculated with and without the dispersion correction.

As can be seen from the data above, the dispersion correction shifts all energies more or less systematically to lower values by 0.1–0.3 eV. As a result, the qualitative picture does not change, and all the discussion presented in the manuscript remains intact.

SII. INFLUENCE OF WATER ON ABSORPTION SPECTRA

As the main optical transitions in hybrid systems are typically due to metal cluster orbitals, theory predicts solvent effects to be minor. [S2, S3] Consistent with this, our test calculations indicate that influence of a solvent on optical absorption spectra (the central property of the current study) is minimal.

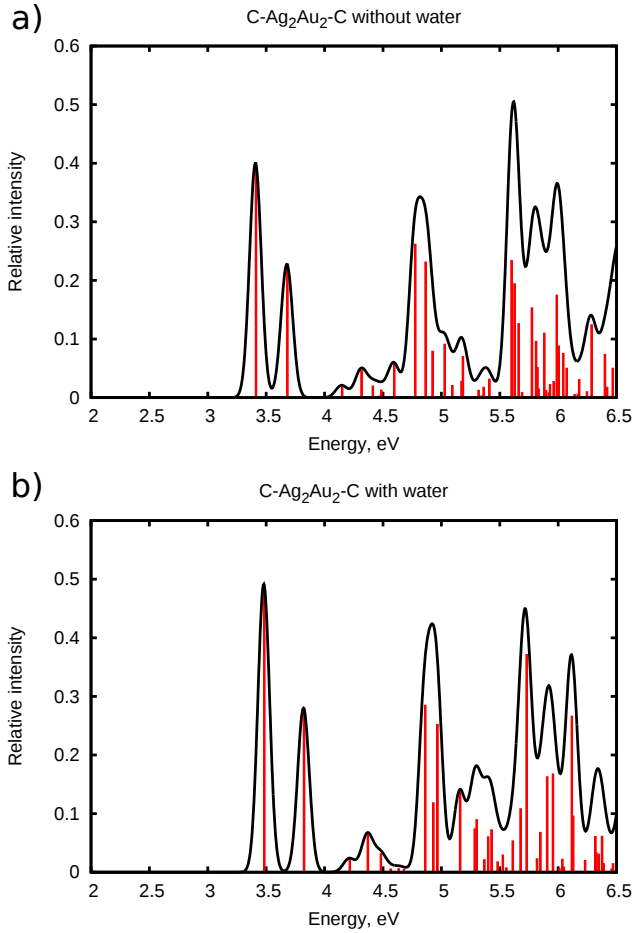

FIG. S1. Optical absorption spectra for C–Ag_2Au_2–C (a) without solvent, (b) with water.

As an example, here we present the optical absorption spectra of the C–Ag_2Au_2–C complex with and without water (introduced as an implicit solvent, as implemented by the PCM model in Gaussian 09). As can be seen from the pictures, the influence of water is not significant.

SIII. OPTICAL ABSORPTION SPECTRA OF INDIVIDUAL CLUSTERS

A. Ag_n clusters

Optical absorption spectra, which were calculated with the `Gaussian 09` package [S4] using the long-range corrected cam-b3lyp functional [S5] and lanl2dz basis set, [S6] compare well to the experimentally observed spectra reported in Ref. S7 (see Fig. S2).

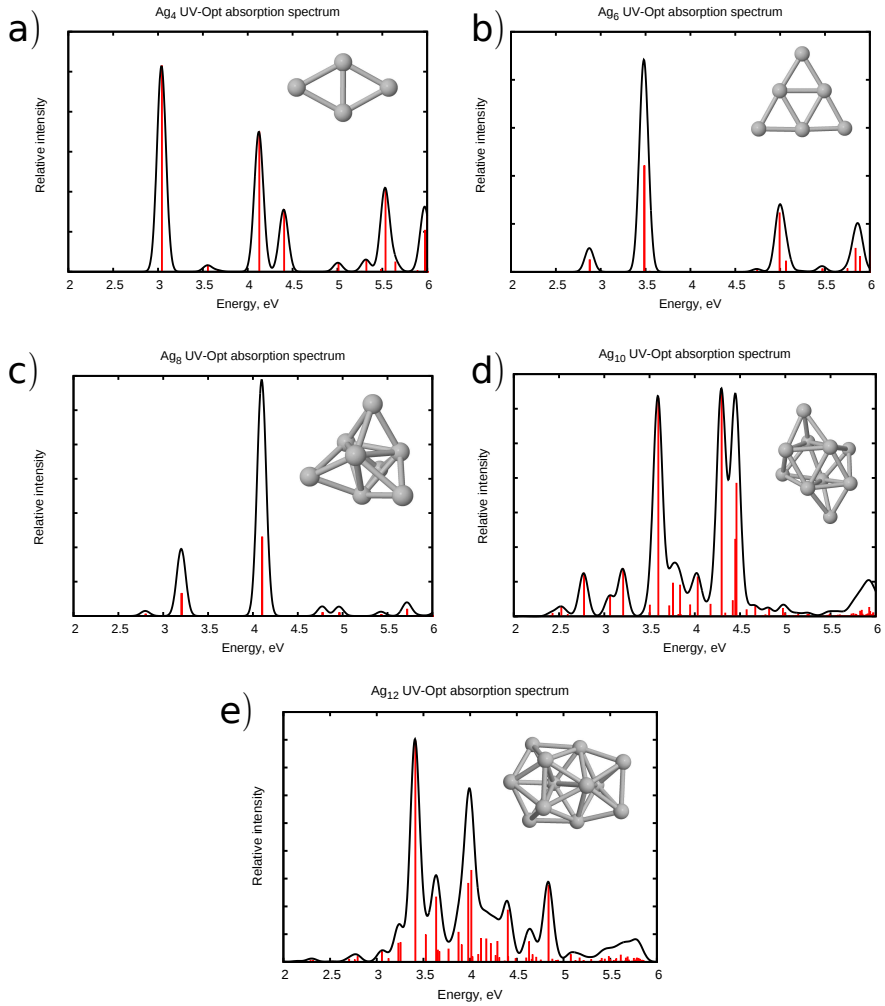

FIG. S2. Calculated optical absorption spectra of (a) Ag_4, (b) Ag_6, (c) Ag_8, (d) Ag_{10}, (e) Ag_{12}.

The experimental spectrum of Ag_8 appears to be a mixture of the two lowest-lying isomers, [S7] although the ground-state structure is evidently responsible for the main spectral features. The best fit with experiment in the case of Ag_{10} cluster is observed for the newly identified C_2 structure, which agrees with experiment much better than the previously suggested D_{2d} isomer. Overall, our computational approach seems to work very well for silver

clusters both in terms of finding the correct global minima, and accurately predicting the corresponding optical absorption spectra.

B. Au_n clusters

The comparison to experimental optical absorption spectra is somewhat more tricky for the Au_n clusters. The Au_4 spectrum agrees well with the experimental results reported in Ref. S8 (Fig. S3, panel a), if one takes into account that experimental spectrum is only recorded up to 5 eV, and that the three experimental peaks between 3.5 and 5.0 eV are somewhat contracted in our calculated spectrum.

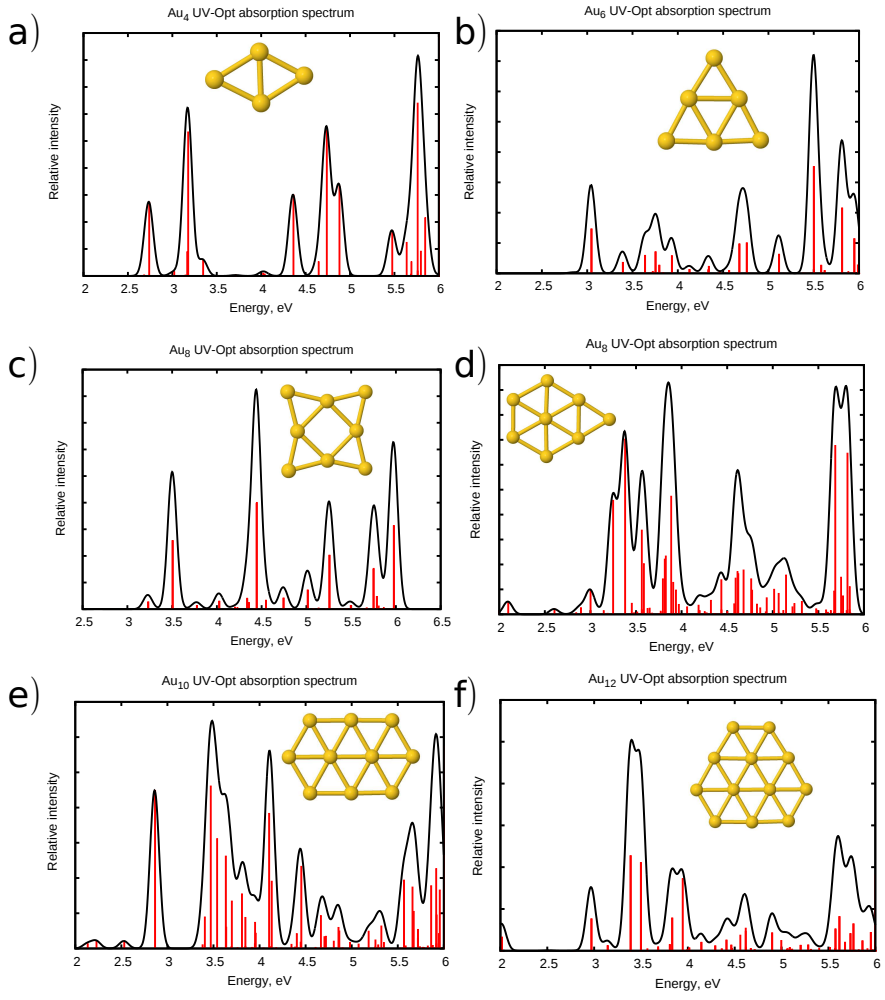

FIG. S3. Calculated optical absorption spectra of (a) Au_4, (b) Au_6, (c) Au_8 (D_{4h}), (d) Au_8 (C_{2v}), (e) Au_{10}, (f) Au_{12}.

For Au_6 (Fig. S3, panel b), the experimental spectra are available for phosphine-stabilized

clusters $[Au_6(PPh_3)_6][BF_4]_2$ [S9] and $[Au_6(Ph_3P(CH_2)_3PPH_2)_4][NO_3]_2$ [S10]. Additionally, a local density approximation computed spectrum is available in Ref. S11. Both available experimental spectra exhibit only a few features in the UV-vis range (200–600 nm or 2–6 eV) that can also be seen in our calculated spectrum.

Experimental data for Au_8 clusters is available for a pure cluster in an ion beam [S8], as well as for a resin-treated gold cluster (Au_8S_n) [S12] and a phosphine-stabilized cluster ($[Au_8(PPh_3)_8][NO_3]_2$) [S10]. Our cam-b3lyp/lanl2dz calculations for the the first low-lying C_{2v} isomer (Fig. S3, panel d) match the experimental data for the isolated Au_8 cluster very well. The spectrum in Ref. S12 shows three peaks at 3.30, 4.82, and 5.48 eV. This agrees reasonably well with the calculated spectrum of the C_{2v} isomer. The absorption spectrum of the phosphine-stabilized Au_8 exhibits similar features, and matches the computed spectrum even better, if one takes into account that the computed spectrum is slightly shifted towards larger wavelengths.

For Au_{10} and Au_{12} we are not aware of any high resolution experimental data. However, our calculations agree well with the results of previous theoretical investigations of Au_{10} and Au_{12} reported in Ref. S11 and of Au_{12} reported in Ref. S13. Additionally, experimental data on thiolated small gold clusters [S14, S15] suggests that Au_{10} and Au_{12} clusters exhibit the main peak features at 3.7 eV and 3.35 eV, respectively. This agrees well with our calculated spectra featuring largest peaks around 3.5 eV (Fig. S3, panels e) and f).

Thus, our calculated spectra for small gold clusters match the experimental data well in the case of isolated gold clusters, and reproduce most of the observed features in the case of the chemically stabilized clusters.

C. Ag_nAu_n bimetallic clusters

Here we reproduce the optical absorption spectra of the pure silver and gold, and alloyed Ag–Au clusters with 4, 6, 8, 10, and 12 atoms, and compare the orbitals involved in the main excitation transition.

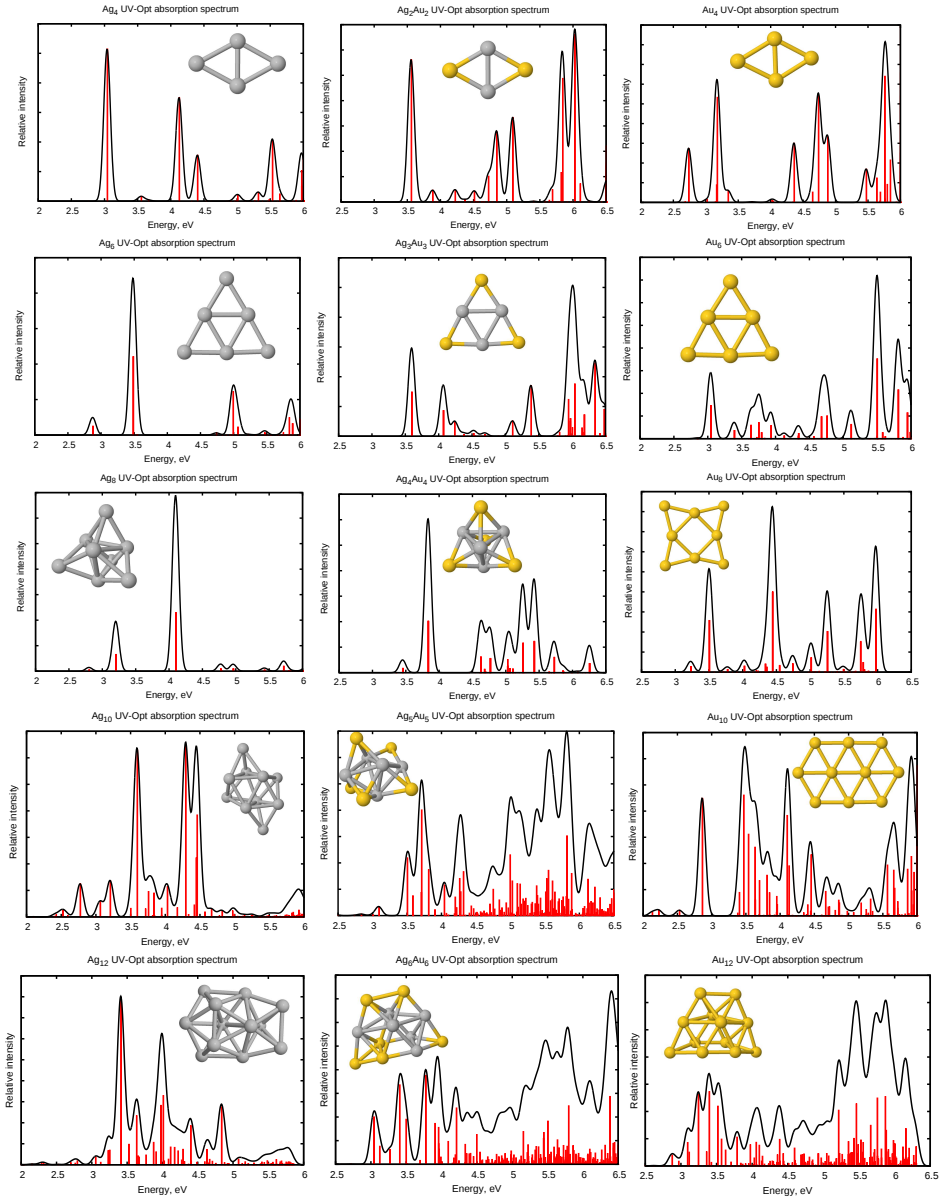

FIG. S4. Comparison of the optical absorption spectra of pure and alloyed clusters. The configuration of the Au_{12} cluster corresponds to the low-lying isomer with geometry matching that of the ground-state structure of the nanoalloy.

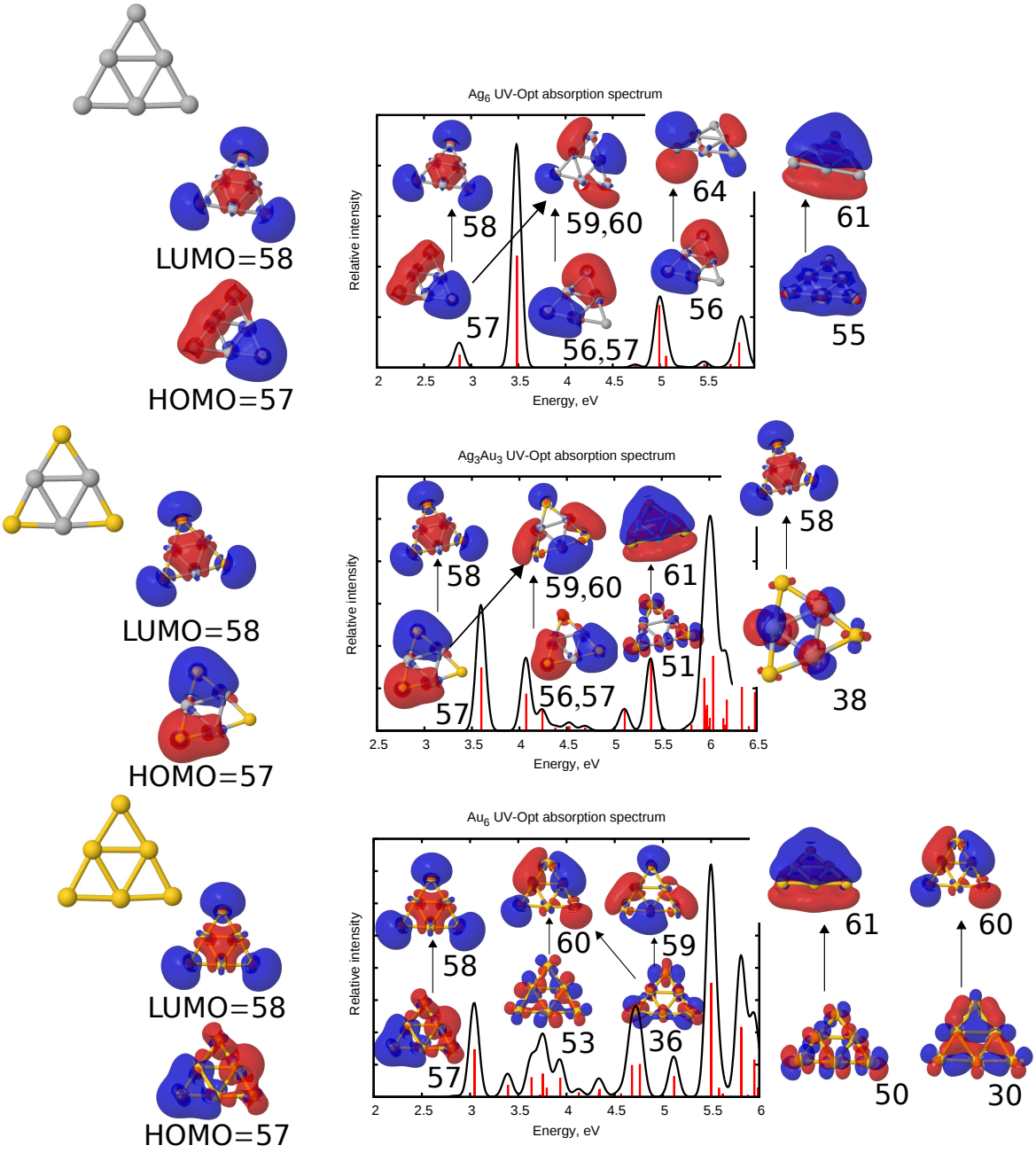

FIG. S5. Comparison of the excitation transitions for (a) Ag_6, (b) Au_6, and (c) Ag_3Au_3.

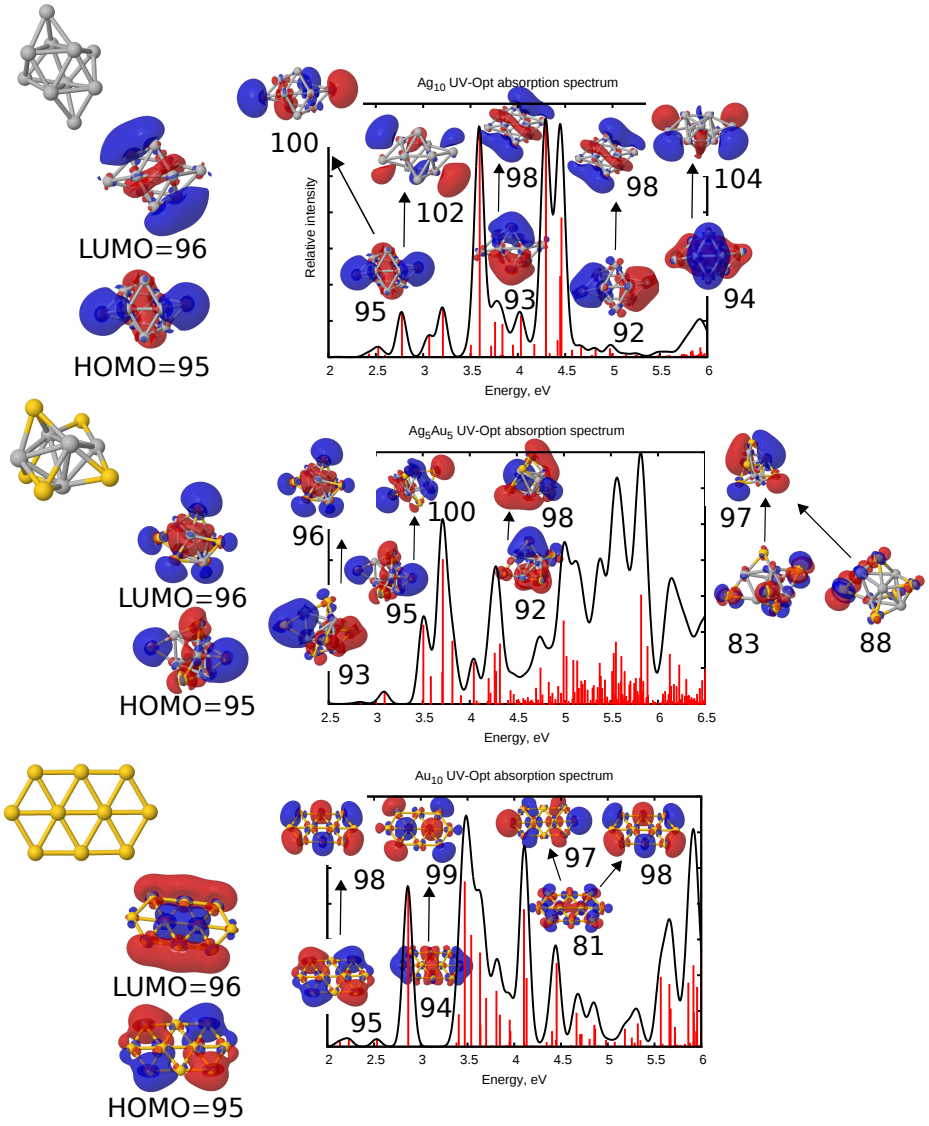

FIG. S6. Comparison of the excitation transitions for (a) Ag_{10}, (b) Au_{10}, and (c) Ag_5Au_5.

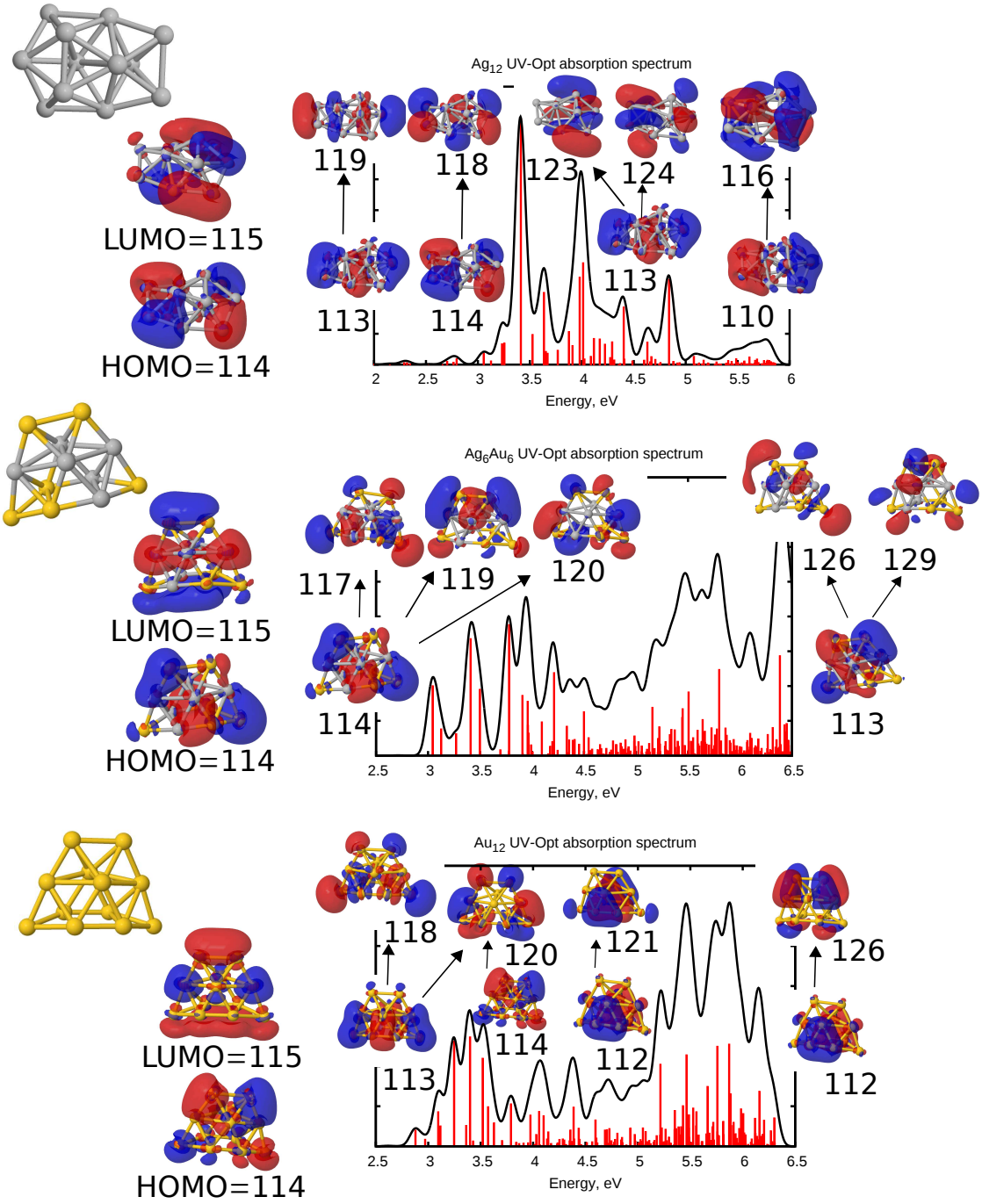

FIG. S7. Comparison of the excitation transitions for (a) Ag_{12}, (b) Au_{12}, and (c) Ag_6Au_6. The configuration of the Au_{12} cluster corresponds to the low-lying isomer with geometry matching that of the ground-state structure of the nanoalloy.

SIV. OPTICAL ABSORPTION SPECTRA OF CYTOSINE-STABILIZED CLUSTERS

Here we reproduce the optical absorption spectra of the individual and cytosine-stabilized clusters, and compare the orbitals involved in the main excitation transition.

A. C–Ag_4–C, C–Ag_2Au_2–C, C–Au_4–C

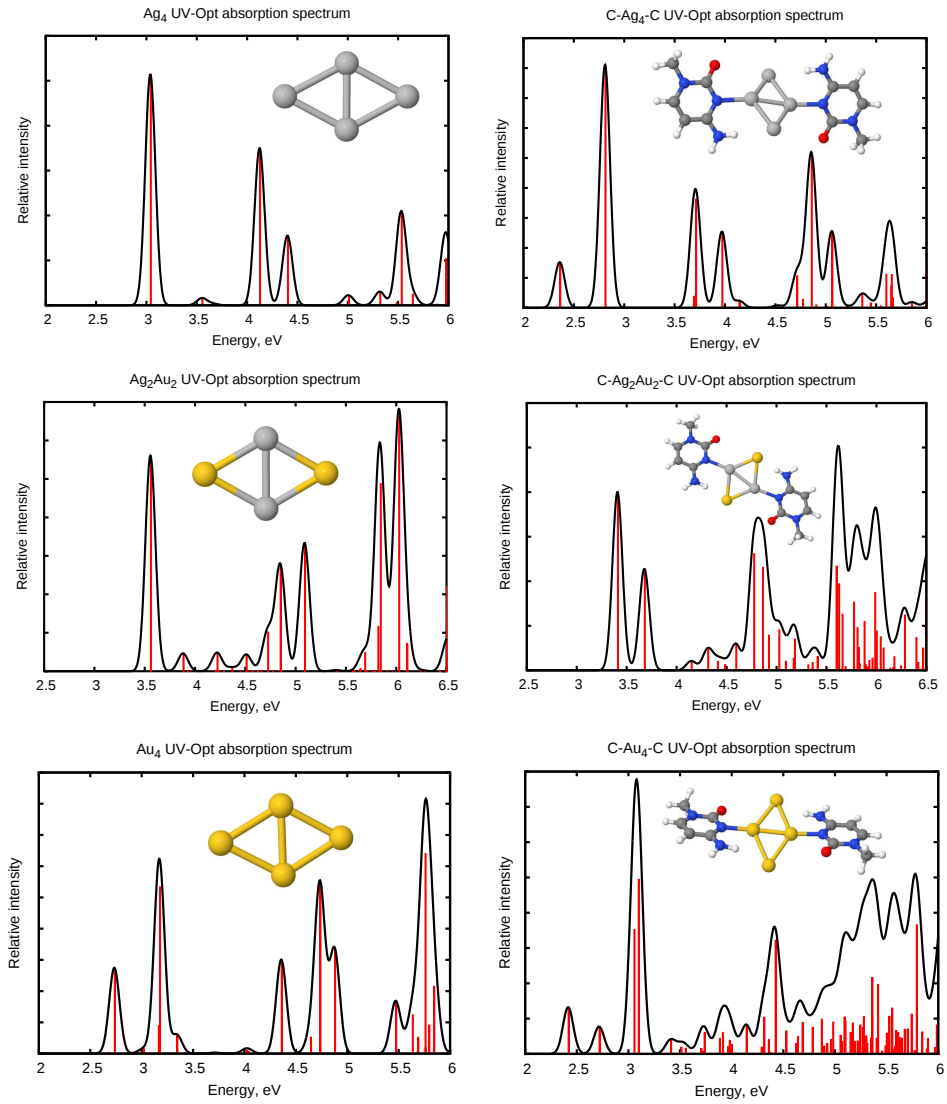

FIG. S8. Comparison of the optical absorption spectra of the individual clusters and clusters associated with two cytosines: Ag_4, Ag_2Au_2, and Au_4.

B. C–Ag_6–C, C–Ag_3Au_3–C, C–Au_6–C

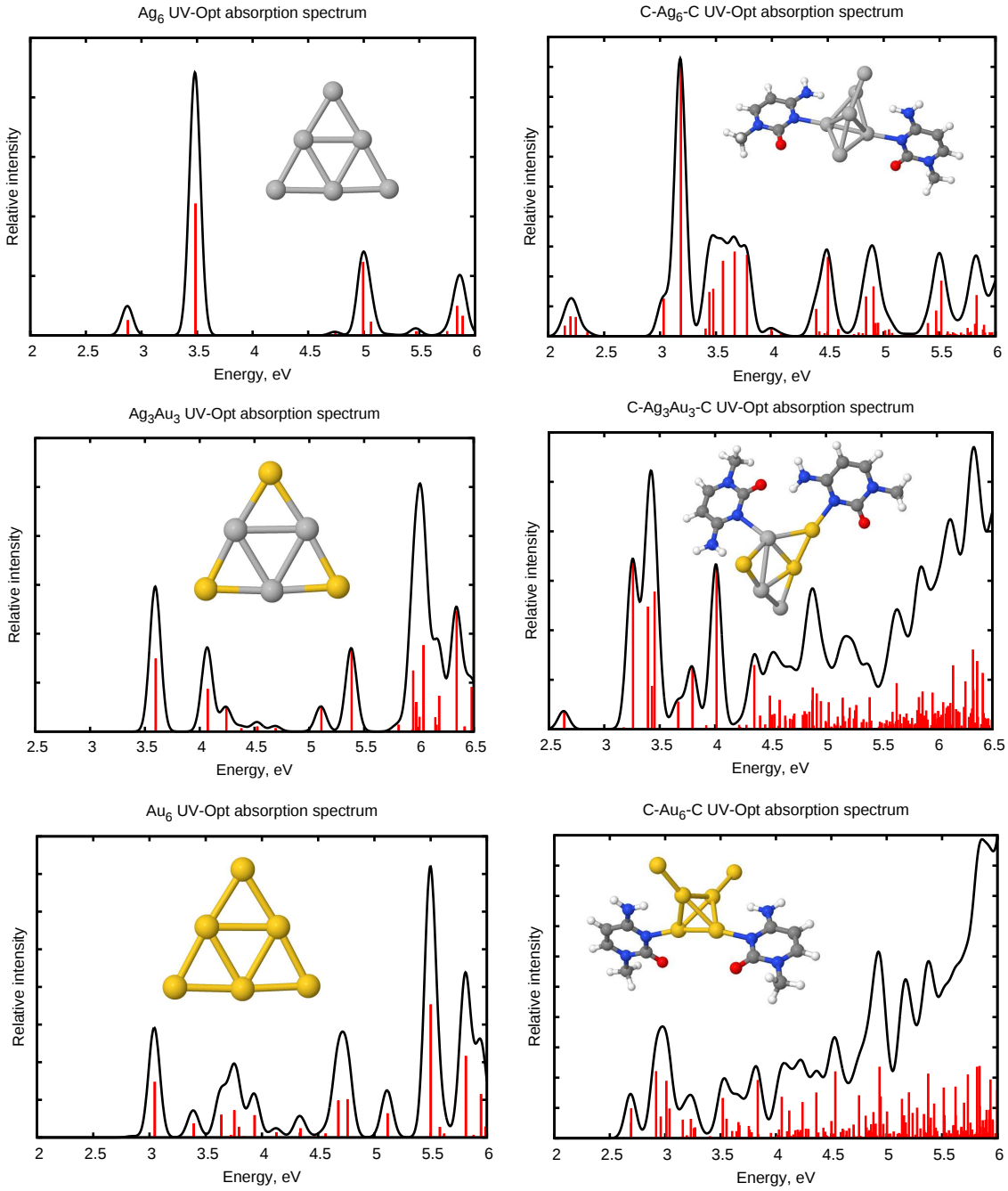

FIG. S9. Comparison of the optical absorption spectra of the individual clusters and clusters associated with two cytosines: Ag_6, Ag_3Au_3, and Au_6.

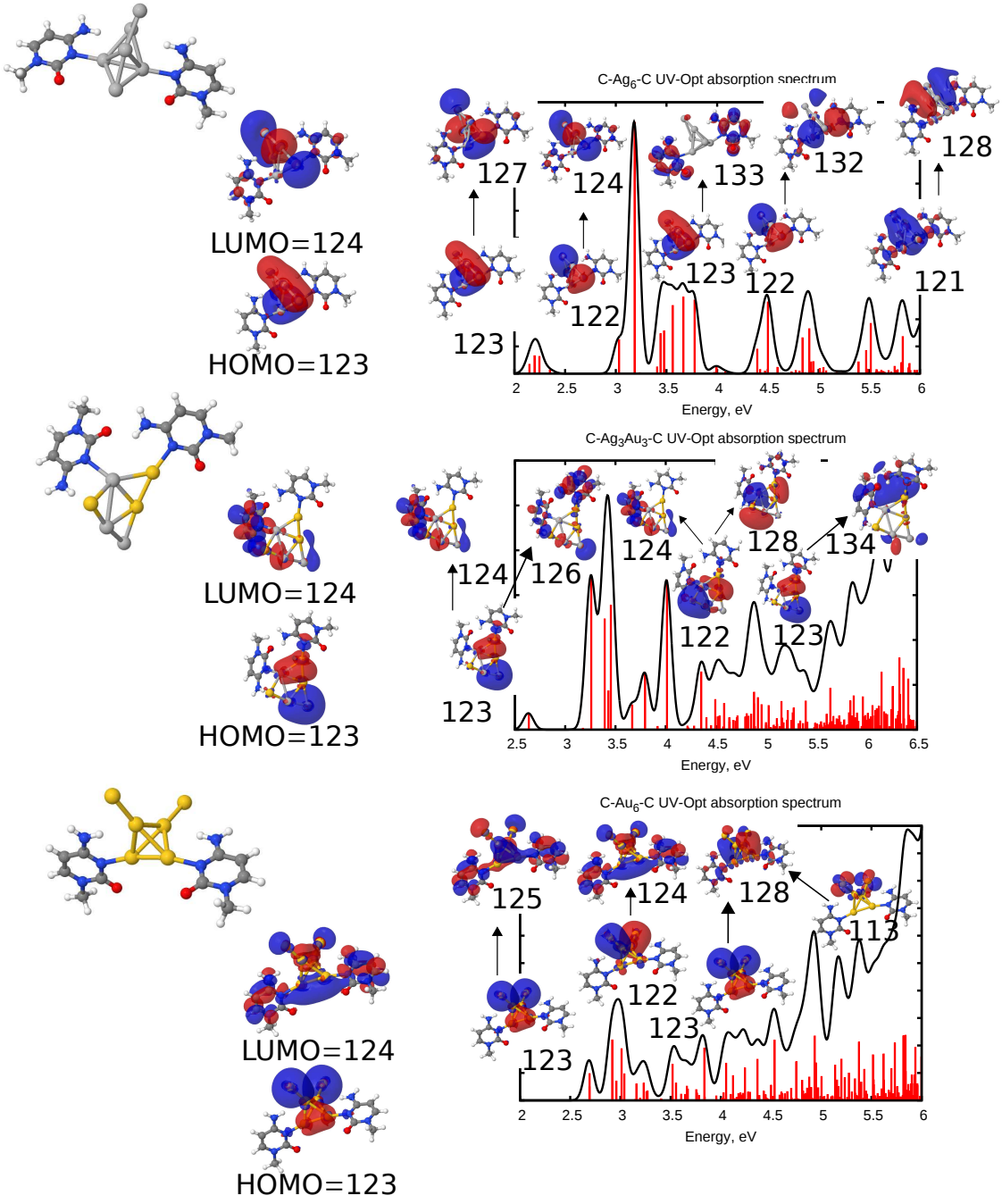

FIG. S10. Comparison of the excitation transitions for (a) Ag_6, (b) Ag_3Au_3, and (c) Au_6 associated with two cytosines.

C. C–Ag_8–C, C–Ag_4Au_4–C, C–Au_8–C

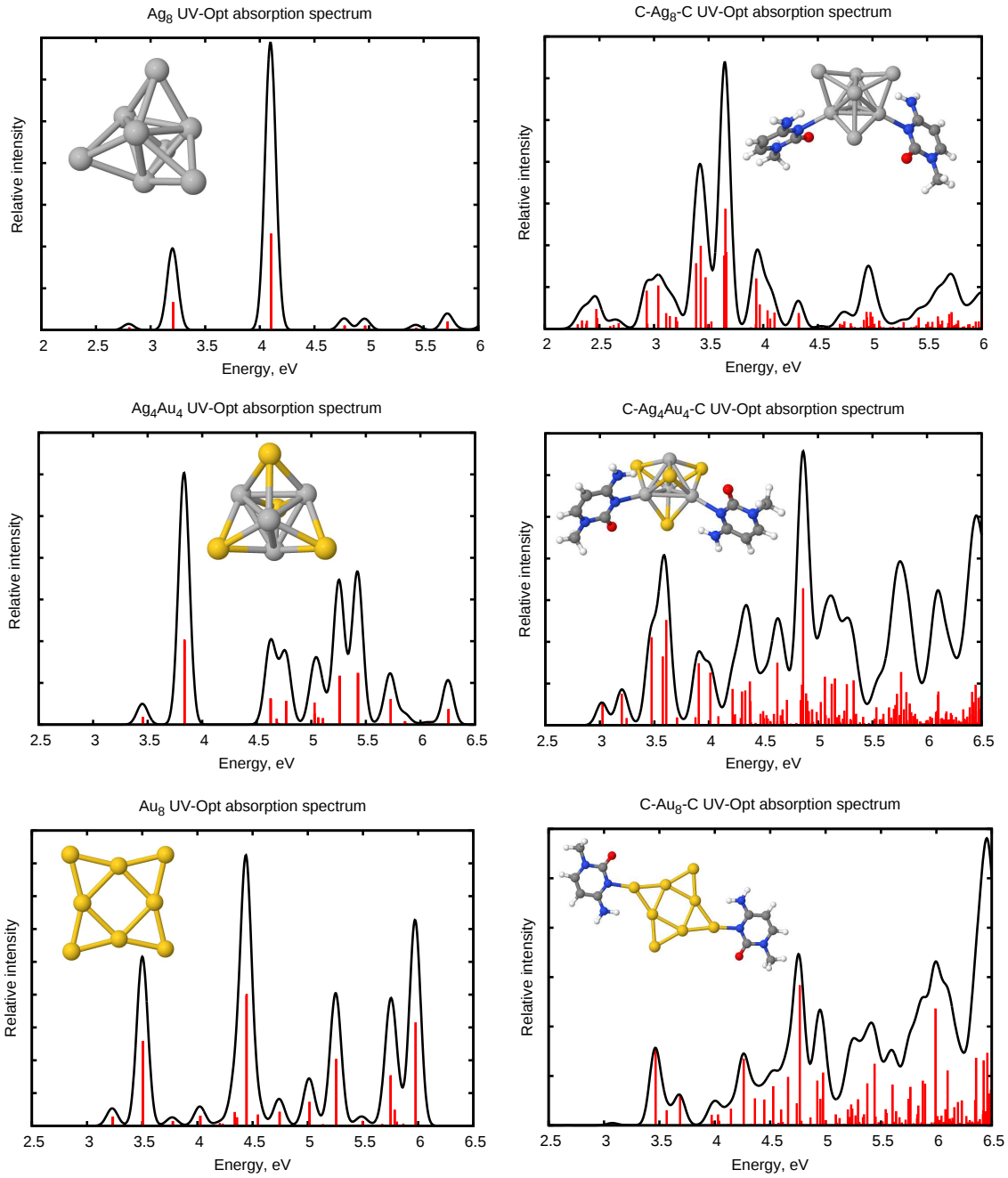

FIG. S11. Comparison of the optical absorption spectra of the individual clusters and clusters associated with two cytosines: Ag_8, Ag_4Au_4, and Au_8.

D. C–Ag_{10}–C, C–Ag_5Au_5–C, C–Au_{10}–C

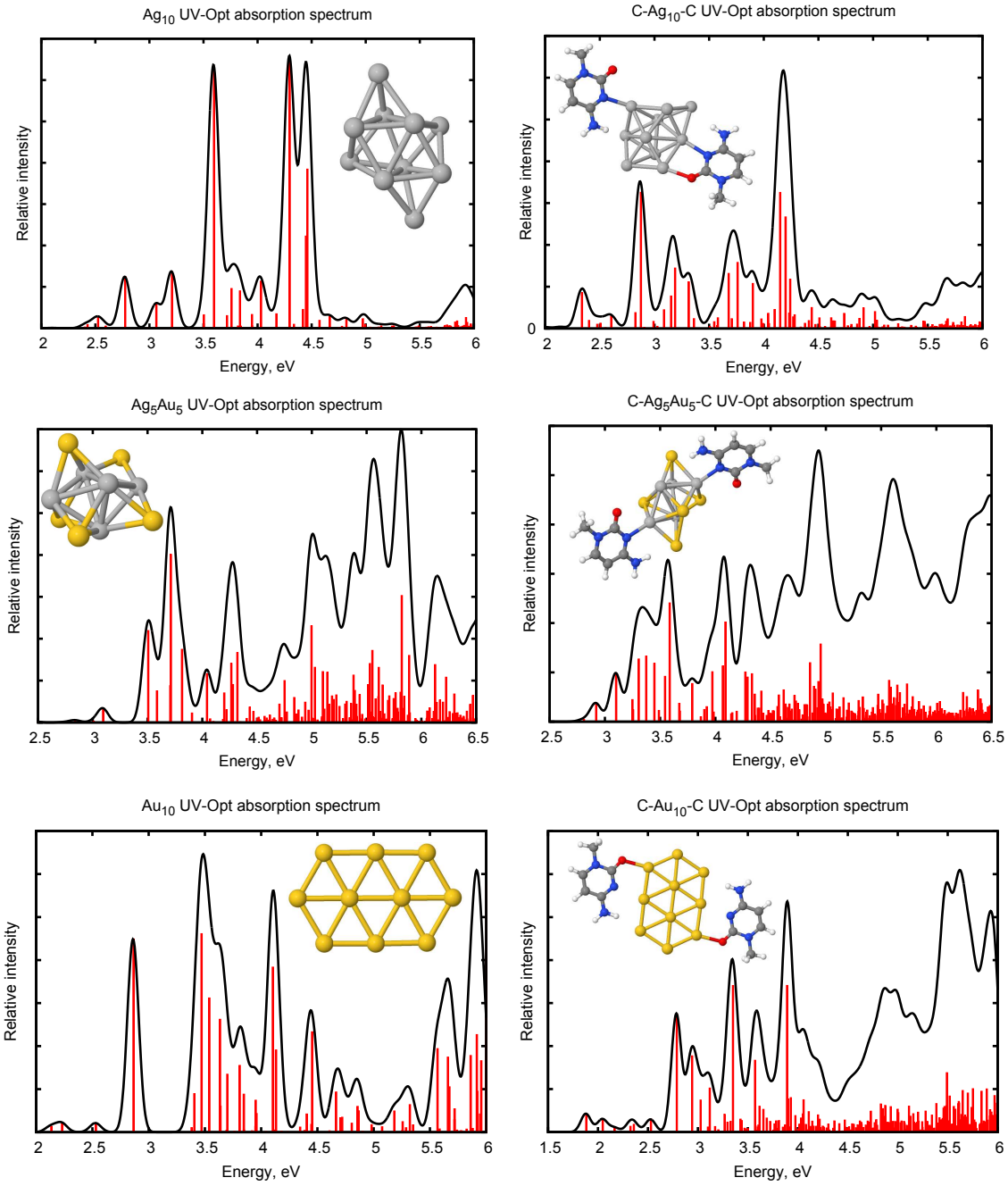

FIG. S12. Comparison of the optical absorption spectra of the individual clusters and clusters associated with two cytosines: Ag_{10}, Ag_5Au_5, and Au_{10}

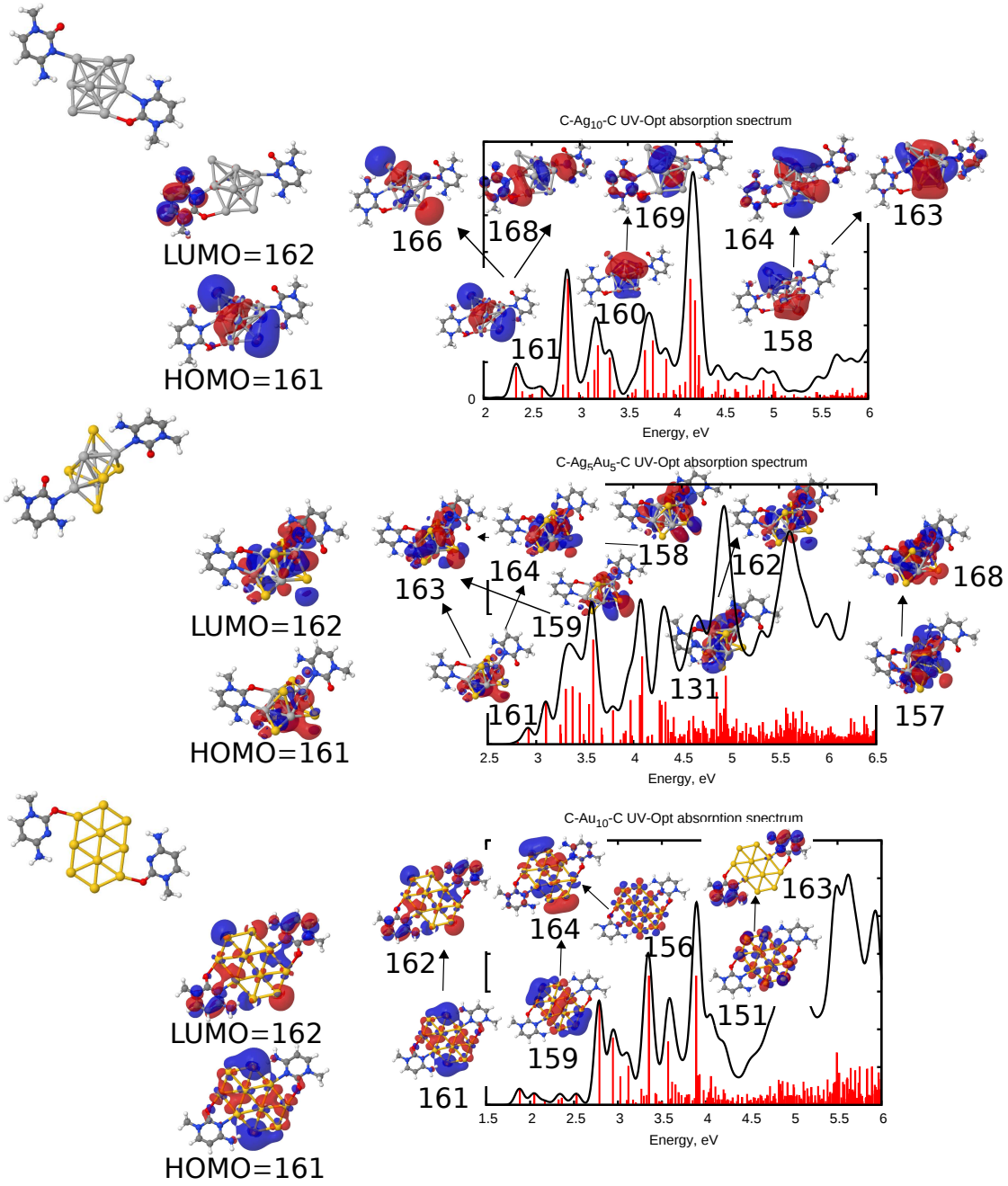

FIG. S13. Comparison of the excitation transitions for (a) Ag_{10}, (b) Ag_5Au_5, and (c) Au_{10} with two cytosines.

E. C–Ag_{12}–C, C–Ag_6Au_6–C, C–Au_{12}–C

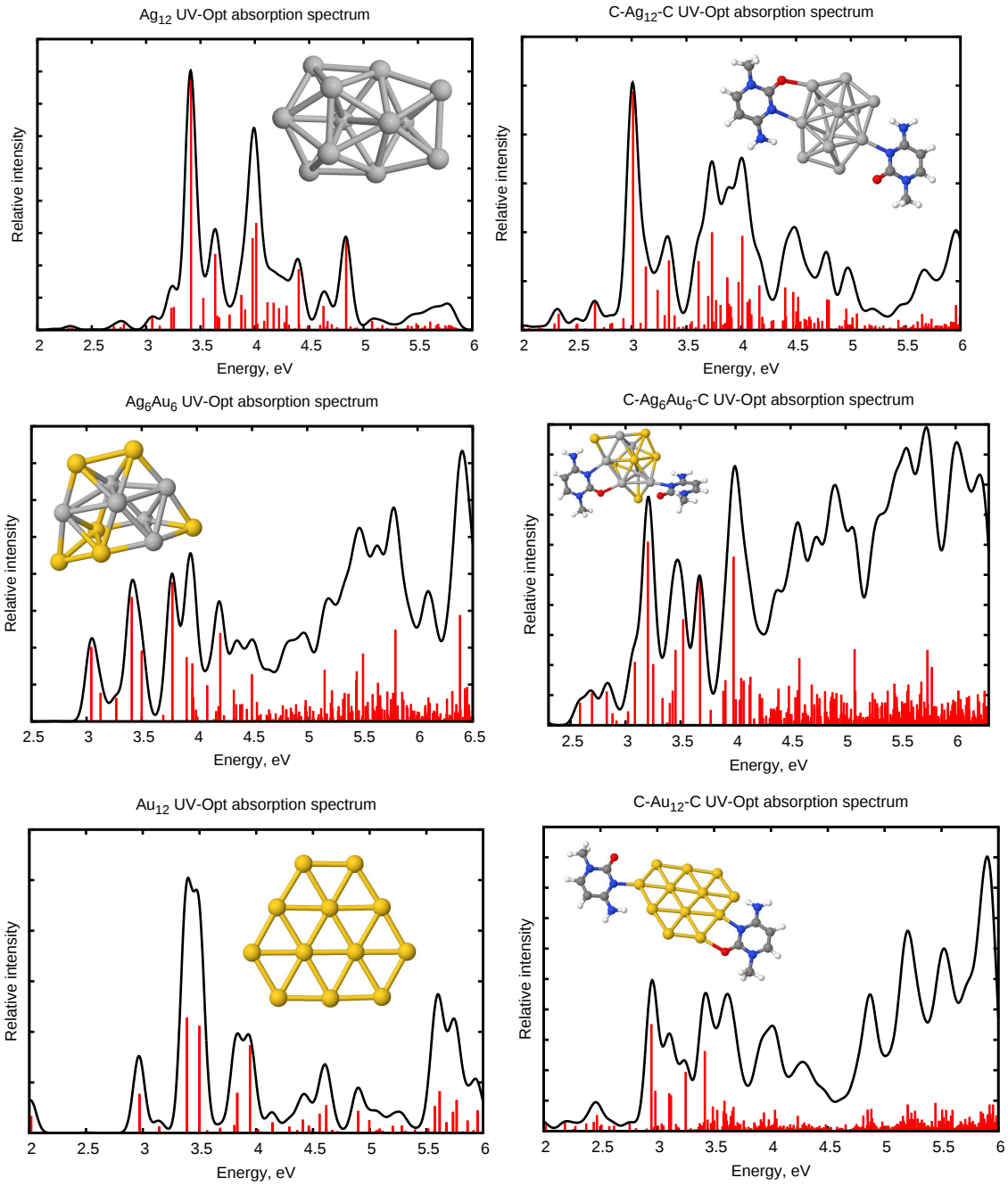

FIG. S14. Comparison of the optical absorption spectra of the individual clusters and clusters associated with two cytosines: Ag_{12}, Ag_6Au_6, and Au_{12}.

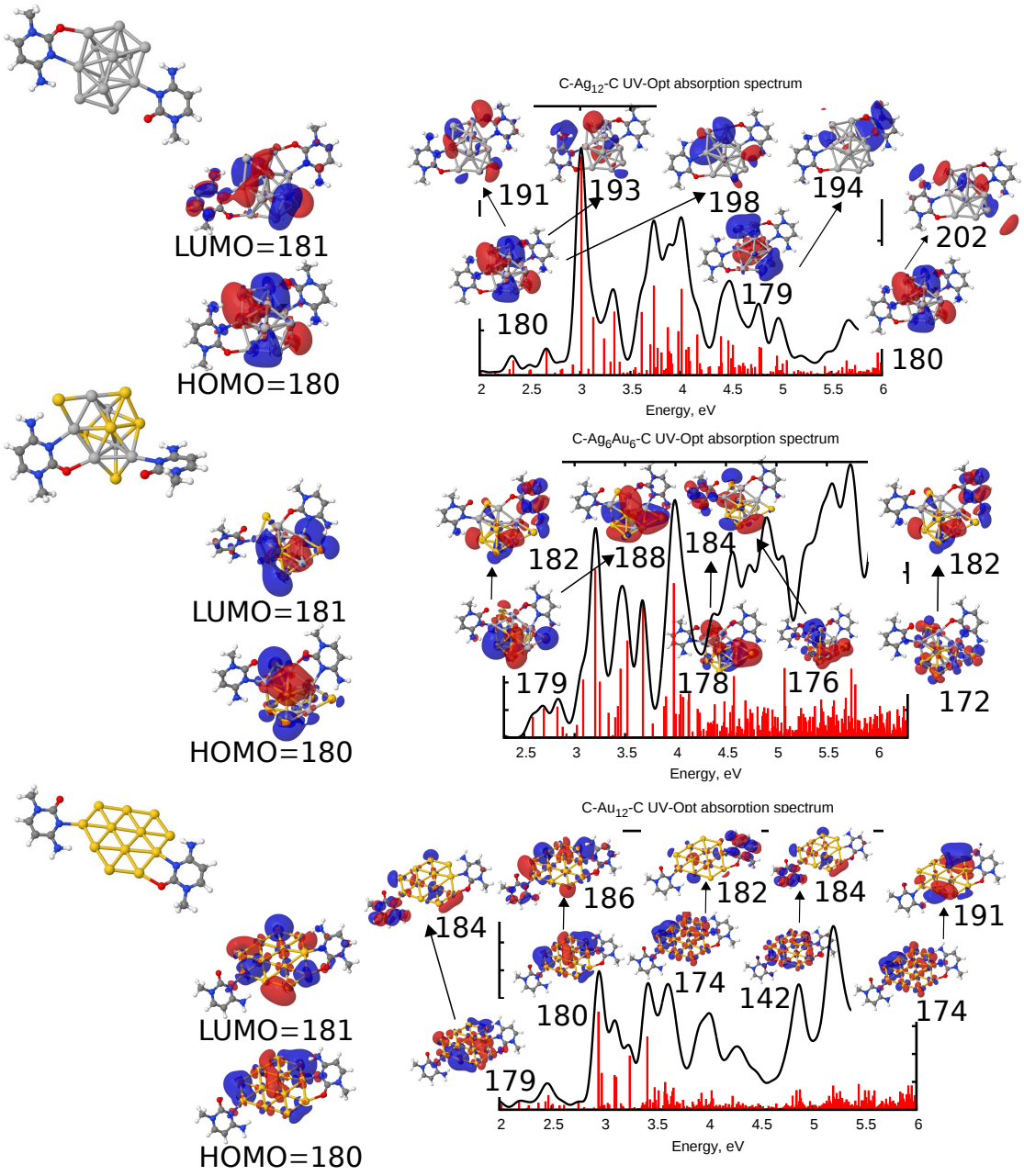

FIG. S15. Comparison of the excitation transitions for (a) Ag_{12}, (b) Ag_6Au_6, and (c) Au_{12} with two cytosines.

F. dC–Ag_4–dC, dC–Ag_4Au_4–dC, dC–Au_8–dC

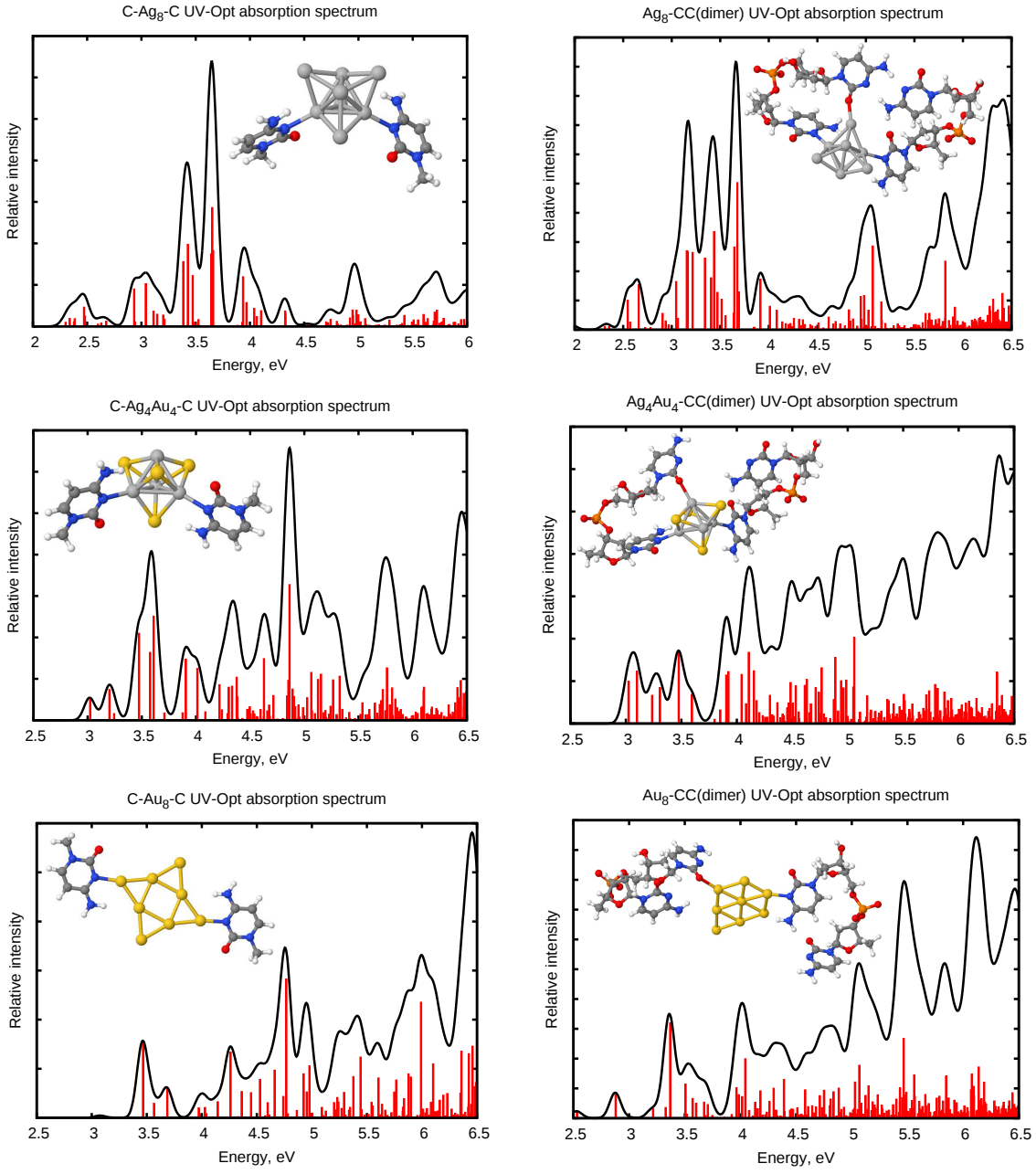

FIG. S16. Comparison of the optical absorption spectra of the eight-atom clusters associated with two cytosine molecules and two cytosine dinucleotides: Ag_8, Ag_4Au_4, and Au_8.

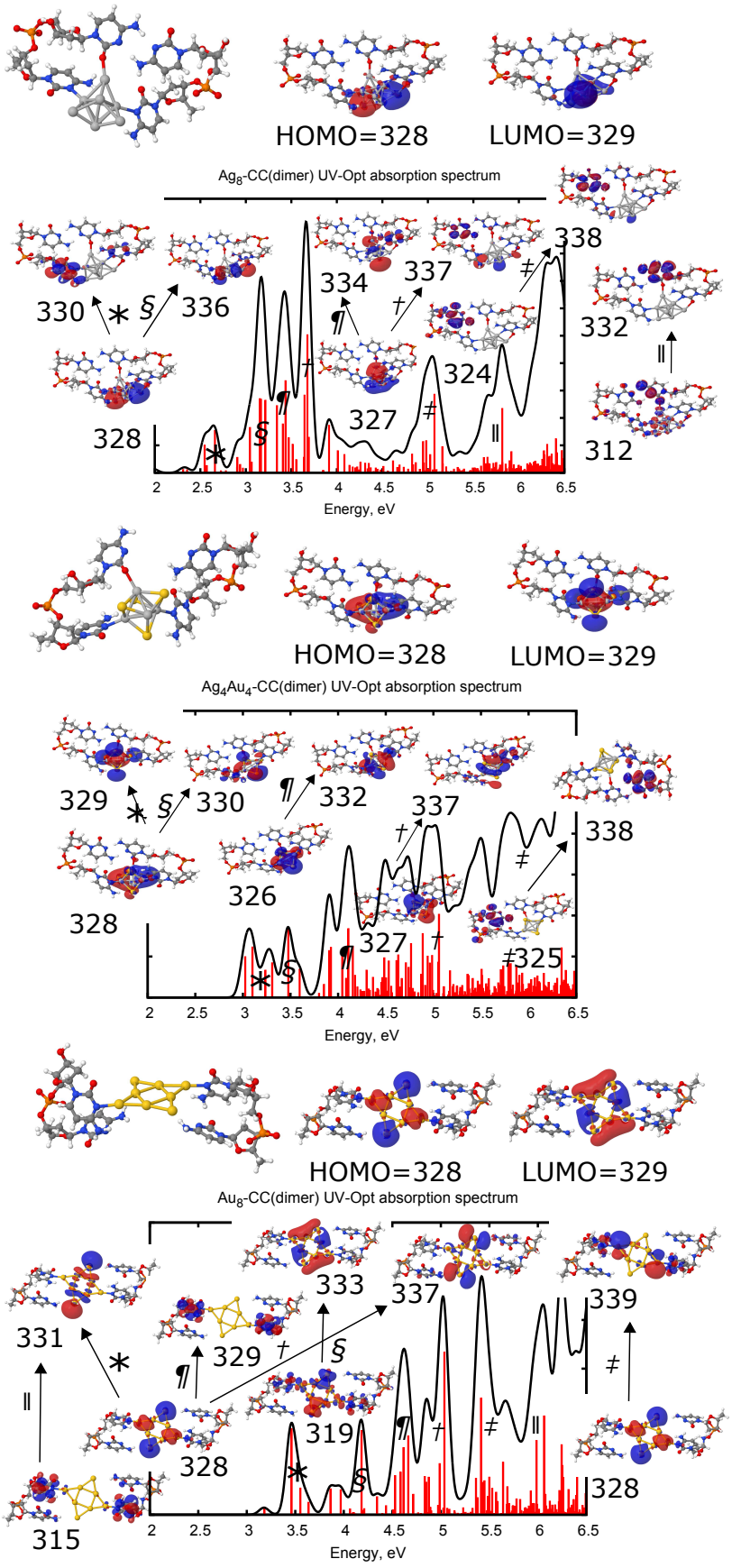

FIG. S17. Comparison of the excitation transitions for (a) Ag_8, (b) Ag_4Au_4, and (c) Au_8 stabilized with two cytosine dinucleotides.

SV. RELATIVE STABILITIES OF HYBRID CLUSTER/DNA AGGREGATES

A. Rod-shaped clusters with hairpin

Local optimization of a higher-lying rod-shaped Ag_4Au_4 isomer (1.63 eV higher in energy than the T_d global minimum, Fig. S18) embedded into a hairpin loop leads to a significant distortion of the aggregate, and destroys the cluster (Fig. S19). With the partial decomposition of the cluster, such configuration turned out to be energetically unfavourable, being 1.39 eV less stable than a rod-shaped cluster isomer and a hairpin individually.

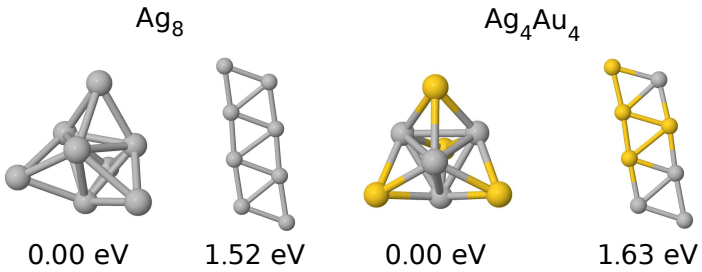

FIG. S18. Rod-shaped Ag_4Au_4 and Ag_8 clusters, and their relative energies with respect to the correspoding ground-state structures.

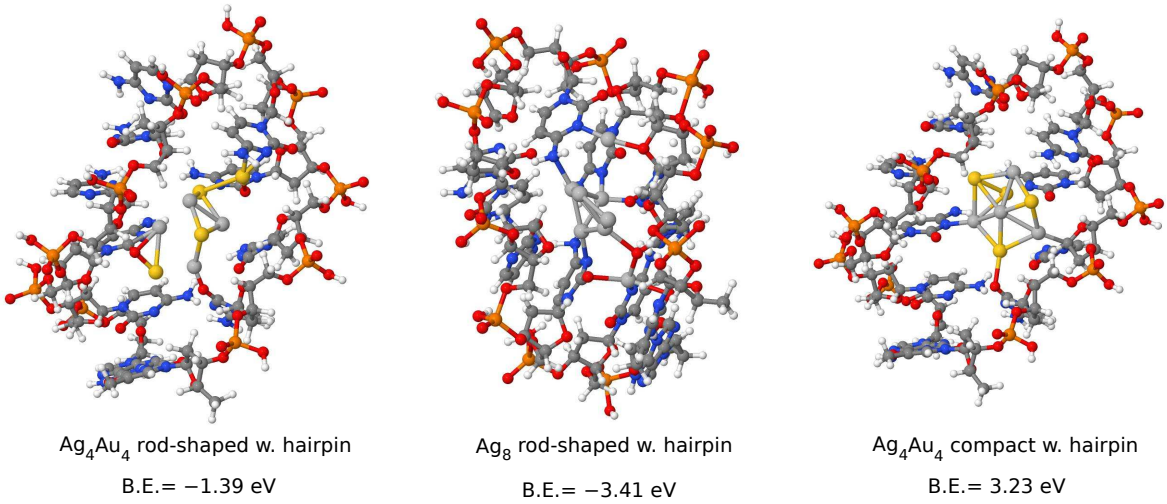

FIG. S19. Rod-shaped Ag_4Au_4 and Ag_8 clusters embedded in a hairpin turned out to be significantly less stable than a compact Ag_4Au_4 cluster.

Curiously, pure silver cluster is even less likely to lead to a thermodynamically stable configuration. In the case of a rod-shaped Ag_8 (1.52 eV higher in energy than the ground-

state structure), the cluster loses two atoms, which are then used to "stitch" the hairpin structure. This leads to a decrease in the hairpin radius, and reorients the cluster into a perpendicular position. The obtained local minimum is significantly higher in energy (3.41 eV) than individual constituent blocks, i.e. an individual hairpin and an individual rod-shaped Ag_8 cluster. Embedding a compact Ag_4Au_4 cluster, on the other hand, is energetically more favourable than keeping a cluster and a hairpin apart.

B. Cluster with duplex

The cluster does not seem to like being embedded into a duplex region, presumably due to steric reasons. The initial configuration with a cluster "forced" inside of the duplex does not converge. Interestingly, embedding is not the only possible scenario of the interaction with the hairpin. An "on the side" position of the cluster can also be achieved for the hairpin. Here, the binding energy is higher than that of the corresponding "on the side" duplex position (0.43 eV vs. 0.12 eV), with the stronger distortion of the DNA fragment observed. This illustrates higher flexibility of the hairpin structure compared to the duplex region.

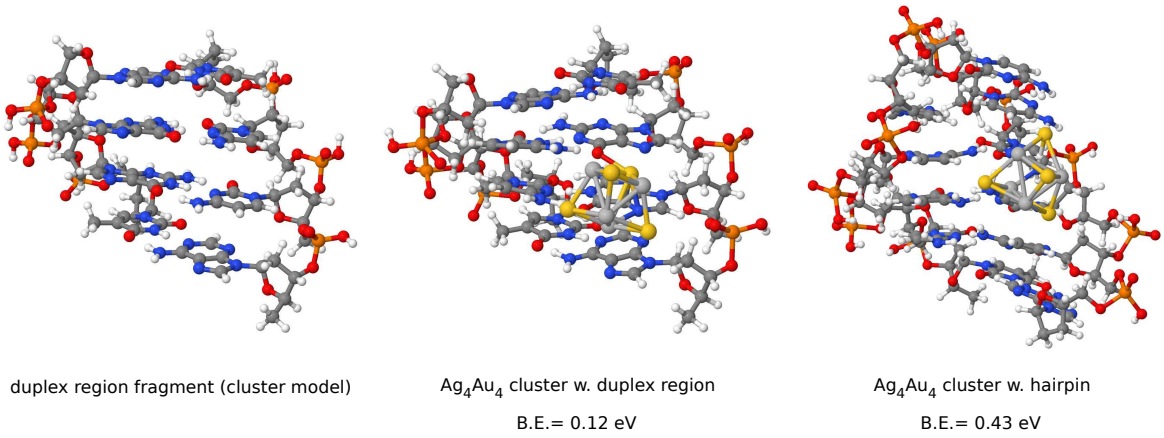

FIG. S20. The Ag_4Au_4 cluster appears to have a very limited tendency to aggregate with a DNA duplex. Ag_4Au_4 can also be weakly bound to the side of a DNA hairpin.

The above data generally supports the original suggestion that the cluster prefers binding to a cytosine-based hairpin, and that the cluster is able to retain its overall compact configuration, thus helping to preserve the main features of the properties of the individual cluster.

[S1] A. Tkatchenko and M. Scheffler, Phys. Rev. Lett. **102**, 073005 (2009).

[S2] C. M. Aikens, J. Phys. Chem. A **113**, 10811 (2009).

[S3] Y. Cui, Z. Lou, X. Wang, S. Yu, and M. Yang, Phys. Chem. Chem. Phys. **17**, 9222 (2015).

[S4] M. J. Frisch *et al.*, Gaussian 09 Rev. D.01, Gaussian Inc. Wallingford CT 2009.

[S5] T. Yanai, D. P. Tew, and N. C. Handy, Chem. Phys. Lett. **393**, 51 (2004).

[S6] P. J. Hay and W. R. Wadt, J. Chem. Phys. **82**, 299 (1985).

[S7] M. Harb, F. Rabilloud, D. Simon, A. Rydlo, S. Lecoultre, F. Conus, V. Rodrigues, and C. Félix, J. Chem. Phys. **129**, 194108 (2008).

[S8] S. Lecoultre, A. Rydlo, C. Félix, J. Buttet, S. Gilb, and W. Harbich, J. Chem. Phys. **134**, 074302 (2011).

[S9] M. A. Omary, M. A. Rawashdeh-Omary, C. C. Chusuei, J. P. Fackler, and P. S. Bagus, J. Chem. Phys. **114**, 10695 (2001).

[S10] J. F. Alvino, T. Bennett, D. Anderson, B. Donoeva, D. Ovoshchnikov, R. H. Adnan, D. Appadoo, V. Golovko, G. Andersson, and G. F. Metha, RSC Adv. **3**, 22140 (2013).

[S11] J. C. Idrobo, W. Walkosz, S. F. Yip, S. Öğüt, J. Wang, and J. Jellinek, Phys. Rev. B **76**, 205422 (2007).

[S12] S. Rath, S. Nozaki, D. Palagin, V. Matulis, O. Ivashkevich, and S. Maki, Appl. Phys. Lett. **97**, 053103 (2010).

[S13] J. V. Koppen, M. Hapka, M. M. Szczęśniak, and G. Chałasiński, J. Chem. Phys. **137**, 114302 (2012).

[S14] Y. Yu, X. Chen, Q. Yao, Y. Yu, N. Yan, and J. Xie, Chem. Mater. **25**, 946 (2013).

[S15] K. G. Stamplecoskie and P. V. Kamat, J. Am. Chem. Soc. **136**, 11093 (2014).